BILINGUAL PUBLISHING GROUP

Journal of Environmental & Earth Sciences

https://journals.bilpubgroup.com/index.php/jees

ARTICLE

Seismic Advance Detection during Roadway Excavation in Underground Coal Mines: Method and Field Applications

Chuanjiu Zhang [1,2]***, Sushe Chen*** [1,2]***, Donglin Fan*** [1,2]***, Fengjuan Tao*** [3*]***, Chunsheng Liu*** [3]

[1] *CHN Energy Shendong Coal Group Co., Ltd., Ordos 01700, China*

[2] *Shendong Coal Branch, China Shenhua Energy Co., Ltd., Ordos 01700, China*

[3] *Wuhan Changsheng Coalmine Safety Technology CO., Ltd., Wuhan 430300, China*

ABSTRACT

Safe and efficient roadway excavation is critical to intelligent coal mine development, while advance geological detection remains challenging under continuous excavation conditions. Conventional advance detection methods often require excavation interruptions, which reduce construction efficiency and limit their applicability in modern intelligent drivage systems. To address this issue, this study proposes a seismic advance detection method conducted concurrently with excavation, utilizing vibrations generated by roadheaders as seismic sources to achieve real-time geological forecasting without interrupting production. A complete processing workflow, including time-window selection, band-pass filtering, first-arrival picking, cross-correlation signal extraction, and depth migration imaging, was developed to extract effective reflection signals from random excavation-induced vibrations and to construct accurate subsurface images ahead of excavation faces. An intelligent while-excavation detection system integrating underground signal acquisition, remote transmission, and rapid interpretation was further established. Field applications were conducted in Roadways 2110 and 2209 of Dongzhouyao Coal Mine under different geological conditions. Results demonstrate successful identification of faults, collapse columns, fractured zones, and lithological transitions ahead of excavation. Imaging results agree well with excavation exposure and drilling verification data, confirming the reliability and practical applicability of the method. The proposed technology enables continuous advance detection during excavation, improves operational safety, and enhances construction efficiency. It shows strong potential for practical application in intelligent roadway drivage and advance

*CORRESPONDING AUTHOR:
Fengjuan Tao, Wuhan Changsheng Coalmine Safety Technology CO., Ltd., Wuhan 430300, China; Email: FJ_Tao@whu.edu.cn

ARTICLE INFO
Received: 26 February 2026 | Revised: 29 April 2026 | Accepted: 6 May 2026 | Published Online: 27 July 2026
DOI: https://doi.org/10.30564/jees.v8i7.12730

CITATION
Zhang, C., Chen, S., Fan, D., et al., 2026. Seismic Advance Detection during Roadway Excavation in Underground Coal Mines: Method and Field Applications. Journal of Environmental & Earth Sciences. 8(7): 261–280. DOI: https://doi.org/10.30564/jees.v8i7.12730

geological hazard prevention in underground coal mines.

Keywords: Intelligent Drivage; Seismic Advance Detection; While-Excavation Monitoring; Geological Anomaly Identification

1. Introduction

The intelligent transformation of coal mines represents a core technological pillar for aligning with modern industrial revolution trends, safeguarding national energy security, and achieving high-quality development in the coal industry. In recent years, China has vigorously promoted the intelligentization of coal mining operations, significantly accelerating the technological upgrading of fully-mechanized mining and excavation faces [1,2]. However, challenges such as confined drivage spaces, demanding construction conditions, and outdated rapid support techniques have resulted in an unclear developmental philosophy for intelligent drivage, coupled with insufficient research on foundational theories and key technologies. Consequently, advance rates often fail to meet production demands, leading to severe imbalances between excavation and extraction activities. Furthermore, as underground roadway drivage is a high-risk zone for safety incidents, achieving safe and rapid roadway development is paramount for the overall intelligent advancement of coal mines.

Within this context of intelligent mining development, geophysical advanced detection technologies play an increasingly critical role in ensuring drivage safety [3–5]. Under conventional mining conditions, the combined approach of comprehensive geophysical surveys followed by verification drilling generally meets the accuracy and predictability requirements necessary for safe production. However, these conventional advanced detection methods are incompatible with continuous excavation activities, significantly impeding operational efficiency [6,7]. The high-speed drivage environment demands real-time, rapid detection and interpretation, rendering traditional detection modes impractical. This discrepancy often pressures mining operations to prioritize progress over essential detection procedures, thereby introducing potential safety hazards. The integration of detection systems directly onto roadheaders, enabling simultaneous while-excavation detection, offers an effective solution to this challenge.

The implementation of detection while-driving eliminates the need for production stoppages, allowing parallel probing and mining operations, which maximizes the productivity of excavation machinery [8]. Moreover, this technology facilitates the continuous acquisition of detection data through real-time dynamic monitoring, and the stacking of multiple detection results enhances overall accuracy [9,10]. In recent years, with the development of geophysical advance detection technologies in underground mines, seismic, electrical, and electromagnetic methods have been widely applied in geological forecasting ahead of excavation [11–13]. Among these methods, seismic methods performed during excavation have become one of the most promising technologies for real-time geological forecasting ahead of tunnel faces [8–10].

Seismic advanced detection technology while driving has been developed from traditional seismic advance prospecting methods. A key distinction lies in the seismic source: traditional methods rely on explosives (posing safety risks, requiring work stoppages, and offering limited range and capability), whereas while-excavation seismic techniques utilize the abundant vibrations generated by the roadheader itself during cutting operations. These vibrations carry substantial energy, representing a highly suitable potential seismic source. Significant contributions have been made in this field: Taylor et al. [14] pioneered the concept of using the roadheader as a seismic source, experimentally validating its feasibility and highlighting its potential as an efficient and low-interference underground detection scheme. Petronio et al. [15] introduced a method employing a near-source signal as a reference trace and applying cross-correlation between this reference and the seismic signals acquired during full-face excavation. This approach effectively extracts meaningful signals and enables fault identification. Lu et al. [16] systematically analyzed the source characteristics of vibrations from shearers, roadheaders, and drills. Their research indicated that shearer vibrations share characteristics with microseismic events, and drill signals exhibit broad-band properties, substantiating the potential of mining machinery vibrations as effective seismic sources. Regarding signal processing and imaging for while-excavation seismic data, Li and Zhang [17] proposed a deconvolution-domain cross-correlation algorithm to transform the random roadheader signals into structured impulsive data. Liu Qiang [18] significantly enhanced signal denoising fidelity and the signal-to-noise ratio using an inverse problem-solving model incorporating L1-norm constraints. Li et al. [10] and Zhang et al. [9] improved signal compression and structural identification accuracy through Wiener filter-constrained deconvolution and pulse-shaping algorithms, respectively.

In summary, extensive research has been conducted on various while-excavation detection methods. Seismic methods are highly sensitive to wave impedance contrasts and are effective for detecting geological structures like faults. This paper presents a seismic advance detection system performed concurrently with roadway excavation for identifying geological anomalies ahead of excavation faces in underground coal mines. Field applications conducted in two roadways of Dongzhouyao Coal Mine validated the system's capability in detecting faults, collapse columns, fractured zones, and lithological transitions. Imaging results show good agreement with excavation exposure and drilling verification results, demonstrating reliable detection accuracy and imaging stability under different geological conditions. The technology exhibits strong repeatability during continuous excavation and shows high consistency with actual geological conditions encountered during drivage, indicating strong potential for practical application in intelligent roadway excavation and advance geological hazard forecasting.

2. Methodology

2.1. Seismic Advance Detection While-Driving

Seismic While-Excavation Advance Detection is based on the principle of seismic wave reflection. As shown in **Figure 1**, when the road-header cuts the coal wall, the generated seismic waves propagate in multiple directions. One part travels directly backward, forming direct waves, which are received directly by the geophones. Another part propagates forward and laterally. When impedance contrast interfaces, such as faults or fracture zones, exist ahead of the excavation face, a portion of the seismic wave energy is reflected back and captured by the geophones. By analyzing these reflected signals, geological anomalies can be inferred.

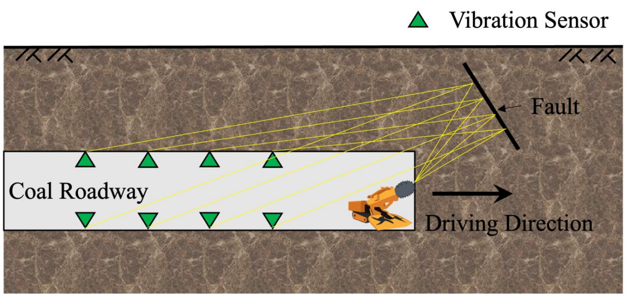

Figure 1. Diagram of seismic advance detection while-driving.

2.2. Seismic Source Generation Mechanism

During the rock-breaking process, the roadheader's cutting head generates an axial force (F_z) in the direction of drivage and a transverse shear force parallel to the tunnel face. These forces are the primary sources of seismic wave excitation. Axial Force F_z: Determined by the working pressure of the telescoping cylinder, this force primarily generates P-waves and the vertical component of S-waves (SV-waves). Transverse Shear Force F_n: Determined by the cutter head's motor power and rotation speed, this force mainly generates the horizontal component of S-waves (SH-waves).

Unlike the instantaneous pulse of an explosive, the roadheader's cutting process is a continuous, pseudo-random, multi-source superimposed seismic source. The roadheader's operating state changes randomly, and other machinery like shuttle cars and conveyor belts also produce continuous vibrations (see **Figure 2**). Spectral analysis of measured signals shows that the roadheader's random seismic source has a wide frequency band, with most energy concentrated between 50 and 150 Hz, which allows for higher resolution detection.

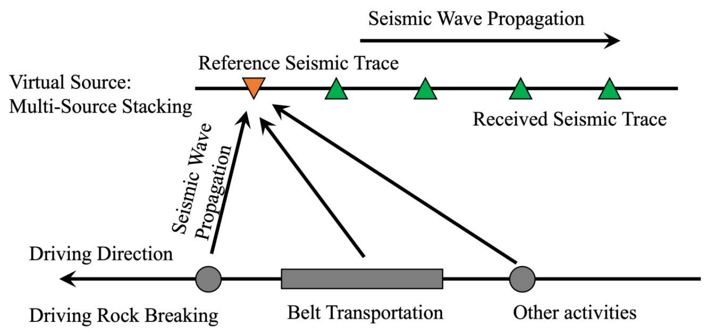

Figure 2. Schematic diagram of excavation-induced seismic source.

2.3. Intelligent Signal Processing

Signal preprocessing is performed to suppress noise and enhance reflection signals prior to migration imaging. To ensure reliable imaging results, raw excavation-induced seismic data are subjected to several preprocessing procedures before cross-correlation processing. These procedures mainly include time-window selection, band-pass filtering, and first-arrival picking, followed by cross-correlation processing to extract effective signals from random excavation sources.

(1) Time Window Selection

In practical measurements, recording length should be adjusted according to exploration objectives and reflection signal quality. Deep reflections usually exhibit weak energy and low signal-to-noise ratios, and excessive recording windows mainly introduce noise while increasing processing time.

Therefore, an appropriate time window is selected to retain useful reflections while compressing unnecessary late-time data. The window length is commonly estimated by:

$$T_d = \frac{L \times 2 \times 2.5}{V_p} \tag{1}$$

Where, T_d is the selected time window length, L denotes the target detection depth, and V_p represents the average P-wave velocity estimated from geological information. Proper window selection improves computational efficiency and data quality.

(2) Band-Pass Filtering

Excavation seismic exploration mainly utilizes reflected waves, while surface waves, refracted waves, and mechanical vibrations act as noise. Band-pass filtering is applied to suppress unwanted frequency components based on spectral differences between useful signals and interference.

Since three-component seismic data contain mixed P- and S-wave energy before wavefield separation, the passband is selected sufficiently wide to avoid loss of useful signals. Appropriate cutoff frequency selection ensures effective suppression of low-frequency noise while preserving reflection information. **Figure 3** compares the signals before and after filtering. It can be seen that filtering significantly improves signal clarity and prepares data for subsequent correlation processing.

(3) First Arrival Picking

First arrivals correspond to direct waves traveling along the shortest path between source and receivers. Accurate picking is essential for velocity estimation and imaging correction.

A sliding-window energy ratio method is adopted due to its robustness and computational efficiency. P-wave arrivals are primarily picked from the X component, where P-wave energy dominates. S-wave arrivals in Y and Z components are approximated using:

$$\frac{V_P}{V_S} = 1.73 \tag{2}$$

where 1.73 is an empirical P-to-S velocity ratio. Manual adjustment may be required when automatic picking deviates from observed phase continuity. Reliable first-arrival picking improves velocity estimation and imaging accuracy.

(4) Trace Energy Equalization

Trace energy equalization is applied to compensate for amplitude variations among traces caused by differences in source coupling conditions, ensuring that the reflection amplitudes primarily reflect subsurface geological structures rather than variations in excitation. The method computes the average amplitude of each trace within a selected time window and then applies a proportional weighting to scale the trace amplitudes, so that the average energy across all traces is approximately equal. This can be expressed as:

$$A'_{i,j} = B_i \cdot A_{i,j} \tag{3}$$

where $A_{i,j}$ is the original amplitude, B_i is the gain factor for the *i*-th trace, and $A'_{i,j}$ is the equalized amplitude.

In the processing workflow, trace energy equalization is typically applied after first-arrival picking. Prior to equalization, high-amplitude near-source traces can dominate the signal, obscuring weaker reflections in traces at larger offsets. After equalization, the amplitudes of all traces are harmonized, reducing the dominance of near-source signals and enabling weak reflections at greater offsets to be more effectively detected, making coherent reflection events more apparent.

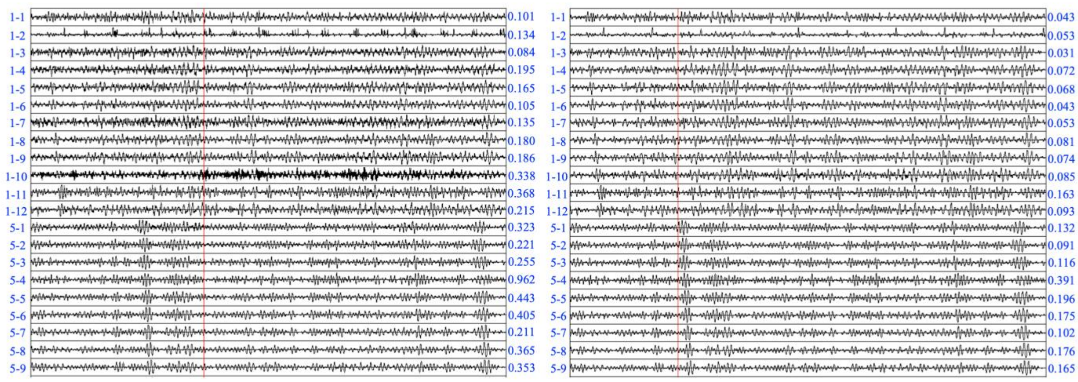

Figure 3. Comparison of signals before and after filtering and first arrival picking.

(5) Cross-Correlation Processing

Cross-correlation is the core of seismic signal preprocessing for random excavation sources and the most commonly used method for extracting effective signals from random signals. Similar to controlled source technology, seismic exploration with random excavation sources requires the collection of reference signals during data acquisition. The cross-correlation technique is then used to process the reference signals and other received signals. Based on the principle of weak signal extraction through cross-correlation, this method can extract weak signals from the cutting head during the tunneling process of the excavation machine. It compresses prolonged seismic signals into pulse signals, enabling the identification of effective signals obscured by noise. Additionally, cross-correlation processing offers a certain filtering effect, effectively suppressing signals unrelated to the reference channel signals, thereby improving the signal-to-noise ratio of downhole testing.

However, the application of cross-correlation in the context of excavation-induced seismic signals exhibits distinct characteristics compared with conventional controlled-source conditions. In roadway excavation, the source is continuously excited by the cutting head, producing signals that are continuous, random, and non-stationary. Meanwhile, as the heading face advances, the relative geometry between the source, receivers, and anomalies continuously changes, requiring multiple sensor relocations and repeated deployments. The same anomaly may manifest different reflection responses at different stages, and the imaging focus varies with the source-to-target distance. These conditions necessitate a targeted adaptation of cross-correlation processing, including reference trace selection, correlation time-window control, and input trace stability management.

In this study, cross-correlation is implemented following raw data editing, adaptive time-window selection, band-pass filtering, first-arrival picking, and trace-energy balancing, serving as a key step to convert continuous random excavation vibrations into interpretable reflection responses. Specifically, time-window selection restricts the correlation to effective signal intervals, reducing contamination from late-arrival mechanical vibrations and unrelated noise; band-pass filtering emphasizes frequency components corresponding to effective reflections; first-arrival picking constrains the time window for relevant signal segments; and trace-energy balancing mitigates the dominance of high-amplitude near-source traces, improving the visibility of weak reflections in the correlated output. The processed cross-correlation results compress the long-duration random vibrations into near-impulse responses, enhancing coherent reflection energy associated with geological interfaces, and provide a stable basis for subsequent velocity analysis, migration imaging, and reflector extraction. **Figure 4** illustrates the signals after cross-correlation pulse processing.

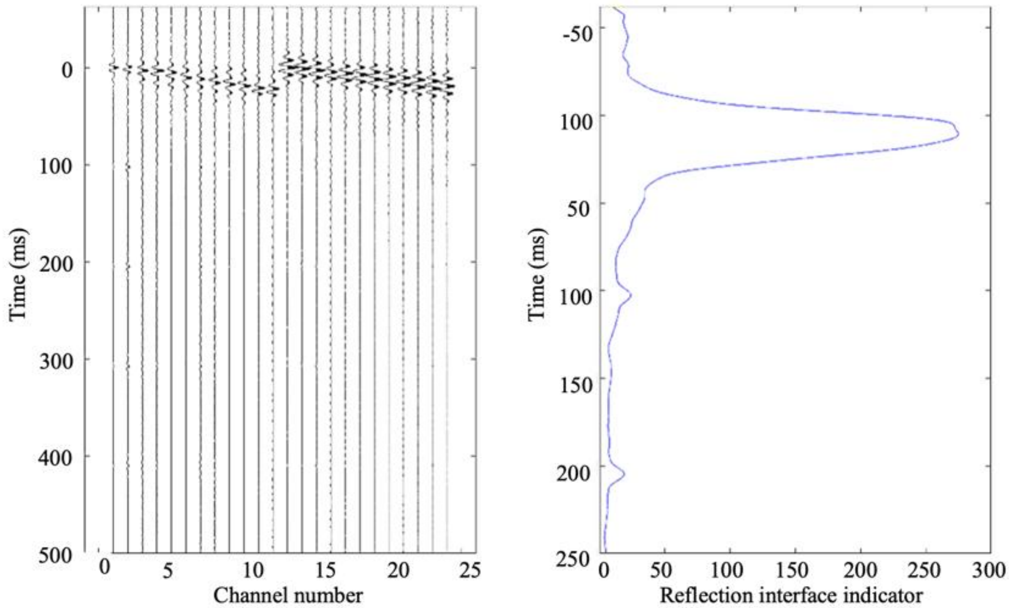

Figure 4. Comparison of signals before and after cross-correlation pulse processing.

2.4. Imaging Method

The key to migration processing lies in establishing a highly accurate velocity model, which is typically an iterative process requiring multiple migration tests. In recent years, prestack depth migration imaging technology has undergone significant development. On the other hand, the current criteria for migration velocity analysis are still largely based on principles proposed in the 1980s, such as the consistency between zero-time imaging depth and zero-offset imaging depth [19,20]. The residual curvature analysis method for common image gather (CIG) flattening and the equal traveltime criterion [21,22]. The velocity analysis procedure in TSPWIN, dedicated software for while-excavation technology, adopts the common image gather flattening criterion. This method closely integrates velocity analysis with migration imaging, ensuring the extraction of relatively accurate velocity information while also suppressing multiples, improving the signal-to-noise ratio, and eliminating the influence of formation dip.

This criterion posits that for a given subsurface imaging point, if the velocity model used for imaging is correct, the imaging results derived from different prestack data should be consistent. The events in the common image gather formed by these results should be flat. If the velocity model is incorrect, the imaging results from different prestack data will be inconsistent, leading to residual moveout in the common image gather. Specifically, overly high imaging velocities cause events to curve downward, while overly low velocities cause them to curve upward.

In tunnel engineering, only the most significant reflection elements are of practical interest. Therefore, corresponding algorithms are used to extract the most valuable P-wave and S-wave reflection surfaces required for construction. This algorithm involves three steps:

(1) Energy compensation balances the energy loss of reflection surfaces. Since Q-value compensation cannot fully offset the loss, the amplitude of different reflection surfaces decreases with distance.
(2) The software simplifies the image as much as possible by ignoring less influential reflection points.
(3) The parameters of each reflection line are calculated, such as size, length, spatial orientation, or the position of the intersection point with the tunnel axis. Reflection elements primarily provide information about structural surfaces at physical boundaries.

The physical properties of reflection surfaces can be represented by wave reflection strength and polarity, generally assessed using the following rules: (a) The stronger the reflection amplitude, the greater the reflection coefficient, and the higher the contrast in elastic wave impedance of the rock medium. Elastic wave impedance is the product of rock density and wave velocity. (b) Red reflection signals indicate positive amplitude, while blue indicates negative amplitude. Positive amplitude suggests a positive reflection coefficient, meaning the rock in front of the reflection surface is hard. Negative amplitude indicates softer rock. (c) Comparing the amplitudes of P-wave and S-wave reflection signals from the same structure helps accurately characterize the reflection surface. Differences between P-wave and S-wave reflection amplitudes help characterize lithological contrasts and fracture development.

When extracting reflection interfaces, parameters should be reasonably selected based on relevant geological data. For example, in areas where the surrounding rock is limestone and karst development is present, the extensibility of karst is limited. In such cases, the extension degree of the reflection axis should be appropriately set to a smaller value during parameter selection.

The key to migration imaging lies in establishing a highly accurate velocity model, which is a typical iterative process requiring multiple migration tests. On the platform of this project, velocity analysis is completed through an iterative operation consisting of four steps:

- Establishing an initial velocity model by estimating direct waves based on picked first-arrival times;
- Defining the detection area and performing grid discretization, then calculating travel times for each grid node using direct wave velocities to create initial travel-time tables for P-waves and converted waves;
- Performing finite-aperture Kirchhoff depth migration based on the initial travel-time tables;
- Updating the velocity model using the common image gather (CIG) flattening criterion as the judgment standard, and reconstructing the travel-time tables.

The updated travel times are then used to perform depth migration again. When the migration results meet the above criterion, the final velocity model and the final migration results are generated as from **Figure 5**. The final result of depth-migrated seismic records appears as a series of elliptical curves, each representing the amplitude image of different reflected signals.

The migration imaging and velocity analysis implemented in this study extend conventional seismic processing methods to accommodate continuous, random excavation-induced sources and dynamically changing source-receiver geometries. Unlike static or controlled-source settings, the workflow integrates iterative velocity model updates with pre-stack depth migration, guided by the common image gather (CIG) flattening criterion. This approach ensures imaging consistency across different pre-stack data, suppresses multiples, and enhances the signal-to-noise ratio under challenging in-situ conditions. Furthermore, the processed reflection surfaces are selectively compensated for energy loss, simplified to focus on the most significant events, and parameterized to provide spatial position, amplitude, polarity, and orientation information, which directly supports geological interpretation and construction planning.

Overall, the imaging results are affected by source characteristics, environmental noise, velocity-model uncertainty, and acquisition geometry. The vibration source generated by the roadheader cutting process is continuous, random, and time-varying, and its energy and spectral characteristics may fluctuate under different operating conditions. Meanwhile, mechanical and environmental noise generated by excavation, transportation, ventilation, and support activities may overlap with the effective wavefield, thereby reducing the detectability of reflected signals. In addition, the construction and iterative updating of the velocity model depend on the quality of first-arrival picking and the reliability of the imaging criterion, while the limited roadway space, restricted receiver aperture, and variable sensor coupling conditions may further increase the instability of the acquisition system. To mitigate these effects, repeated data acquisition was adopted to improve statistical stability, reference-trace cross-correlation was used to suppress random interference unrelated to the seismic source, and preprocessing procedures including time-window selection, band-pass filtering, first-arrival picking, and trace energy equalization were applied to enhance the separability of effective reflections. Furthermore, the velocity model was iteratively updated using the common image gather flattening criterion in order to reduce the impact of uncertainty on the final imaging results as much as possible.

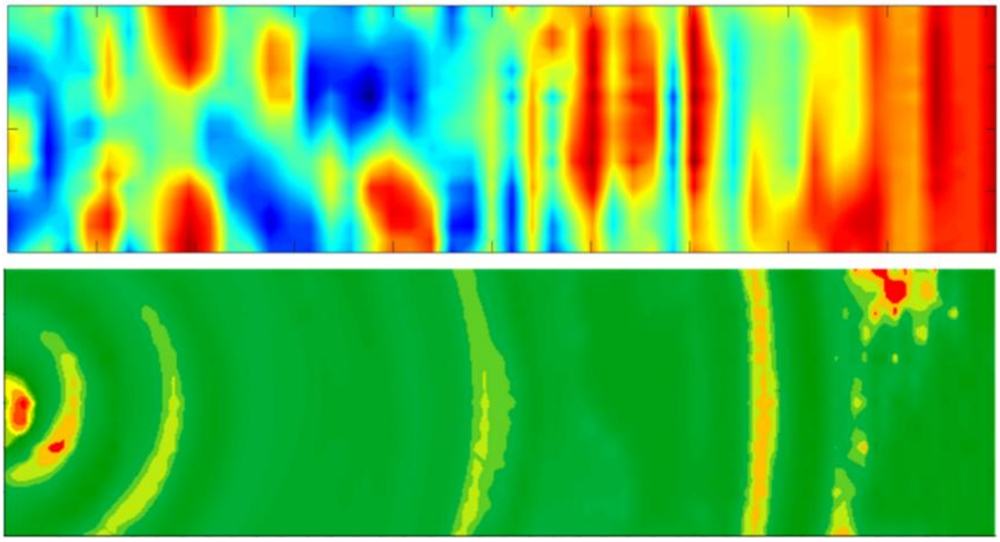

Figure 5. Comparison of imaging results before and after migration processing.

3. Intelligent Advance Driving Detection Prototype System Design

3.1. System Composition and Working Principle

By utilizing contrasts in elastic wave impedance of coal and surrounding rock, a physical basis is established for detecting geological structures ahead of the excavation face. Seismic elastic wave methods are highly effective in identifying geological structures in underground environments.

In this study, vibrations generated by the roadheader during cutting operations are used as seismic sources. When these continuous vibration waves encounter interfaces with acoustic impedance contrasts in the surrounding rock, reflected waves are produced. By recording and analyzing these reflections, geological structures located ahead of and beside the roadway can be detected and interpreted.

This approach provides technical support for intelligent remote-controlled advanced geological detection during roadway excavation. The intelligent remote-controlled while-excavation advanced geological detection system is illustrated in **Figure 6**. As shown, seismic vibration sensors are deployed along both sides of the roadway and connected to multiple detection host units to acquire vibration signals generated at the excavation face in real time. The collected data are transmitted from underground to the surface office through IoT communication systems, after which the intelligent while-excavation advanced detection platform performs rapid processing and imaging to obtain geological information ahead of the excavation face. When unfavorable geological structures, such as fractured zones, are detected, early warnings can be issued promptly.

The remotely controlled while-excavation advanced geological detection system mainly consists of one detection host unit, two vibration sensors, and an intelligent comprehensive analysis platform. The while-excavation detection host unit is a mine-use intrinsically safe portable device designed for underground operation. Its primary function is to acquire voltage signals output by vibration sensors and display them in real time on an LCD interface. Signals collected from each sensor are transmitted and conditioned through operational amplifiers and transmission circuits. After initial signal conditioning, channel gains can be adjusted, typically providing approximately tenfold amplification through selectable circuit configurations to accommodate varying signal strengths encountered in field conditions.

The vibration sensors used in the system are mine-use intrinsically safe electrical devices capable of converting three-component ground velocity signals into corresponding voltage outputs. These sensors operate reliably in hazardous underground environments containing methane and coal dust explosion risks and provide essential input data for subsequent signal processing and geological interpretation.

The intelligent analysis platform is primarily used for processing and interpreting detection data to identify unfavorable geological structures ahead of excavation faces. While-excavation seismic detection is a branch of geophysical exploration adapted for underground engineering applications. This method features long detection range, strong resistance to electromagnetic interference, and clear waveform characteristics, making it effective for identifying faults, fractured zones, goafs, and other structural anomalies. Core modules include signal preprocessing, velocity analysis, migration imaging, reflector extraction, and 3D visualization.

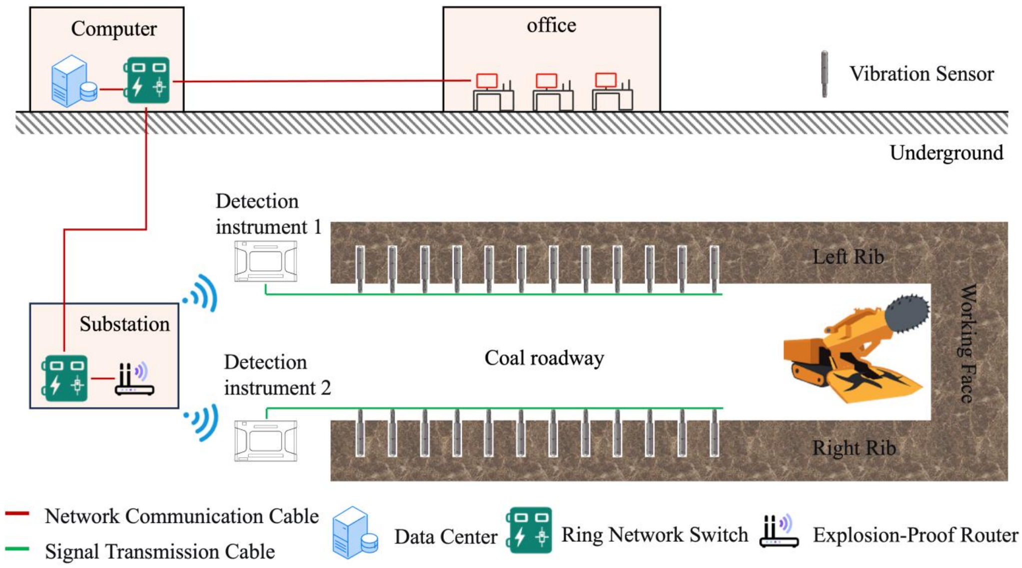

Figure 6. Intelligent advance driving detection prototype system and detection diagram.

3.2. Sensor Array Layout

To achieve continuous geological advance detection during roadway excavation, the receiver array should be dynamically deployed and relocated as the heading face advances. Considering the limited underground space, the continuously changing source position, and the complexity of field construction conditions, a double-row receiver array deployed along the two roadway sidewalls was adopted in this study. The layout procedure is described in **Figure 7** as follows.

(1) Field inspection and determination of the initial deployment position. Before sensor installation, the heading-face position, roadway cross-sectional conditions, rock-bolt distribution, and surrounding-rock stability are first examined, and the distance between the heading face and the existing monitoring array is measured. Based on these field conditions, the initial sensor group is installed at approximately 20 m behind the heading face so as to balance near-source signal strength, receiver coverage, and field safety requirements.

(2) Receiver array deployment. The receiver array is arranged symmetrically along the left and right sidewalls of the roadway. A total of 24 geophones are deployed, with 12 receivers on each side. The channel spacing is controlled within 2–4 m according to the local rock-bolt distribution and field conditions. All geophones are firmly coupled to the coal wall or surrounding rock through rock bolts to ensure stable signal acquisition.

(3) Cable laying and fixation. After sensor installation, signal cables are laid separately along the two sidewalls and fixed to the mesh or support structures in order to reduce the influence of construction disturbance and cable loosening on signal quality. This arrangement also facilitates repeated relocation of the receiver array during continuous excavation.

(4) Sensor positioning and coordinate definition. To facilitate subsequent data processing and imaging interpretation, a unified coordinate system is established. The geophone closest to the heading face is defined as the zero point of the X-coordinate, and the roadway advance direction is taken as the positive X-direction. The Y-coordinate uses the roadway centerline as the reference zero, with sensors on the two sidewalls located on

opposite sides of the centerline, while the Z-coordinate is defined based on a unified elevation reference. After coordinate definition, all sensors are numbered and their spatial positions are recorded.

(5) Dynamic relocation of the receiver array. As the heading face continues to advance, the distance between the original receiver array and the seismic source gradually increases. When the heading face is approximately 80 m away from the first sensor group, the near-source signal energy decreases significantly and the effectiveness of reflection-wave recording is correspondingly reduced. In this case, the sensors and signal cables are removed and reinstalled at a new position about 20 m behind the updated heading face, using the same deployment scheme as the initial array. By repeating this procedure, the receiver array can move synchronously with the advancing heading face, thereby forming a continuous while-excavation monitoring mode.

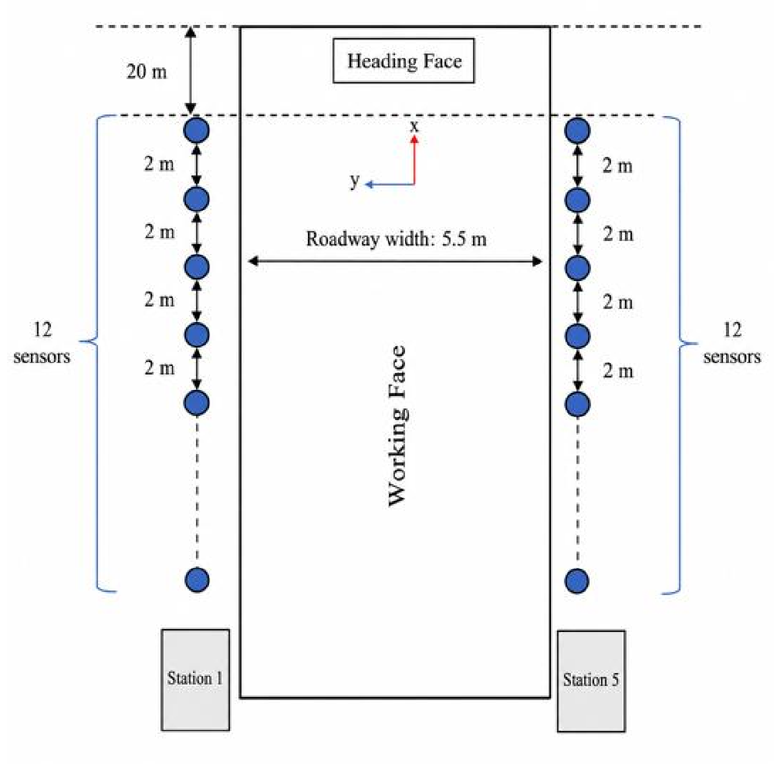

Figure 7. Schematic diagram of double-row sensor layout for while-excavation geological advance detection.

Through the above layout procedure, the receiver array can be maintained within a reasonable distance behind the excavation face, ensuring effective acquisition of near-source vibration signals and providing a stable data basis for subsequent cross-correlation processing, velocity analysis, migration imaging, and reflector interpretation.

3.3. Observation Procedure and Dynamic Relocation Strategy

In this study, the excavation-induced vibration generated by the roadheader cutting process is used as the seismic source, without interrupting excavation for additional artificial excitation. This observation mode allows seismic data to be acquired simultaneously with roadway excavation, thereby improving operational efficiency and meeting the requirement of continuous advance detection under active construction conditions.

During data acquisition, the deployed geophones continuously record vibration signals generated by the cutting process. Each individual dataset is acquired for approximately 2–5 min, and multiple datasets can be recorded depending on data quality and field conditions. In general, a total acquisition duration of about 30 min is considered appropriate to balance data quality and construction efficiency. The recorded signals are transmitted through the underground acquisition system and subsequently uploaded to the intelligent analysis platform for further processing.

By combining excavation-induced source recording with dynamic receiver-array relocation, the observation procedure enables the acquisition system to remain closely coupled to the advancing excavation face. This provides a stable and continuous data source for subsequent signal preprocessing, cross-correlation-based reflection extraction, velocity analysis, migration imaging, and reflector interpretation, thereby supporting real-time geological forecasting during roadway excavation.

4. Field Application

This study conducted advance detection during roadway excavation at Dongzhouyao Coal Mine, where two roadways (Roadway 2110 of Panel 1 and Roadway 2209 of Panel 2) were selected for field application and validation of the proposed detection technique. The investigations targeted typical underground geological conditions, including lithological variations, fractured zones, and broken or isolated rock blocks, in order to evaluate the reliability and practical performance of the method in underground mining environments. Detailed results and analyses for the selected roadways are presented in the following sections.

4.1. Advance Detection in Roadway 2110 of Panel 1

4.1.1. General Information

A series of advance detection experiments during excavation was conducted in Roadway 2110, which is located in Panel 1 of the No. 4 coal seam at Dongzhouyao Coal Mine, China. Surface elevations range from 1,391 to 1,418 m, while the roadway elevation lies between 902 and 914 m, corresponding to a burial depth of approximately 489–504 m. The ground surface is characterized by loess-covered hilly terrain with locally developed gullies and no permanent surface water bodies, resulting in limited direct influence on underground operations. The roadway has a designed length of approximately 1,030 m with a cross-sectional dimension of 5.5 m × 3.6 m. Adjacent areas include previously mined panels, while portions of overlying Jurassic seams have experienced historical mining disturbance; however, due to the large interlayer distance, their influence on the current excavation area remains limited.

The 2209 roadway is situated in the No. 4 layer of the Permian lower Shanxi Formation's first district. The coal seam is a composite seam with a total thickness ranging from 3.31 to 11.43 meters and an average thickness of 7.37 m. It has 2 to 4 layers of gangue, with an average thickness of 0.46 m. The coal seam dip is gentle, generally ranging from 1° to 3°, with an average inclination of approximately 2°. The immediate roof mainly consists of interbedded mudstone and fine-grained sandstone, locally intercalated with conglomeratic sandstone, while the main roof is dominated by fine- to silt-grained sandstone. The floor strata are composed primarily of silty mudstone and fine sandstone, underlain by medium- to coarse-grained sandstone. Geological structures in the panel are relatively simple, although localized normal faults and collapse columns may be encountered, where surrounding rock fracturing tends to intensify and requires strengthened support measures. Detailed information on the lithological characteristics and physical-mechanical properties of the coal seam roof and floor is provided in **Table 1**.

Table 1. Roof and Floor Characteristics of Coal Seam of 2110.

Layer	Rock	Thickness (m)	Lithology Description	Compressive Strength (MPa)
Old Roof	Fine-grained sandstone, siltstone	4.45–4.7, average 4.58	Fine-grained sandstone: Gray to grayish-white, fine-grained, massive. Siltstone: Gray, silty. Contains a small amount of mica debris, with a horizontal layered texture.	34.15
Direct Roof	Interbedded mudstone, fine-grained sandstone, sandy conglomerate	4.45–6.52, average 5.47	Fine-grained sandstone: Gray to grayish-white, fine-grained, massive. Sandy conglomerate: Grayish-white, with coarse sand and small gravels (0.20–0.50 m).	64.25
Direct Floor	Silty mudstone	0.32–9.11, average 4.72	Mudstone: Gray to dark gray, contains clay. Siltstone: Grayish-white, silty.	34.97

Table 1. *Cont.*

Layer	Rock	Thickness (m)	Lithology Description	Compressive Strength (MPa)
Old Floor	Fine-grained sandstone, sandy mudstone, silty fine sandstone	3.40–6.08, average 4.44	Fine-grained sandstone: Grayish-white, fine-grained, massive. Coarse-grained sandstone: Grayish-white, with a coarse-grained texture.	51.00

Geological structures within the panel are relatively simple, but localized faults and collapse columns are predicted along roadway development. The 2110 roadway revealed two normal faults, with displacements of 1.5 and 9.0 m. Observations from adjacent workings indicate gentle seam occurrence with locally developed fractures. Several small normal faults with throws generally less than 10 m may be encountered, and surrounding rock fracturing tends to intensify near structural zones, requiring strengthened support during excavation. Within the detection section of Roadway 2110, a fault structure crossing the roadway was identified, as illustrated in **Figure 8**. The fault trends obliquely across the roadway alignment and intersects the haulage gateway approximately 81.41 m ahead of the reference point M16 of the detection section.

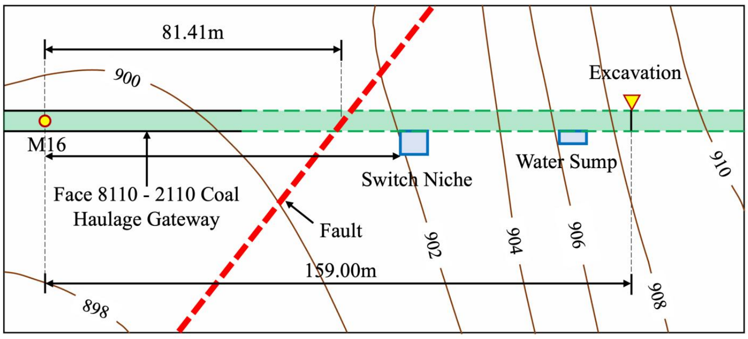

Figure 8. Detection test design and layout of Face 8110-2209 roadway.

Hydrogeological conditions are classified as moderately complex, with the primary water sources being sandstone fracture water in the roof strata and possible water accumulation in nearby mined-out areas. Surface water influence is negligible, while Ordovician limestone aquifers beneath the seam exhibit weak water-bearing properties with sufficient aquiclude thickness separating them from the working seam. Calculated water inrush coefficients remain below critical thresholds, indicating overall safe mining conditions, although localized structural zones may still serve as potential water-conducting pathways.

4.1.2. Advanced Detection Design

During the initial on-site installation, the first sensor on each side was mounted on the sidewalls approximately 20 m from the excavation face. Subsequently, additional sensors were installed against the direction of excavation at intervals of one rock bolt, meaning the actual spacing between sensors varied based on the on-site rock bolt spacing. The coordinates of each sensor were measured and recorded after installation. The schematic layout of the sensors is shown in **Figure 8**.

As the tunnel advanced and the distance between the excavation face and the first set of sensors increased, leading to weakened signal reception, the equipment was relocated and reinstalled approximately 20 m from the new excavation face. In the 2110 tunnel experiment, sensors were installed five times. The relocation points, based on tunnel advancement milestones, were at chainage 750, chainage 813, chainage 843, chainage 907, and chainage 951. The specific X-coordinates of the sensors for these three installations are listed in **Table 2**. A total of 24 receivers were arranged with a channel spacing of 2 m. Sensors connected with detection instrument L or R have a Y-coordinate of 2.75 m and −2.75 m, respectively. The Z-coordinate uses the center of the tunnel height (or the datum line) as the reference zero point. The geophones were coupled to the coal wall by mounting them on rock bolts. The observation system is illustrated in **Figure 9**. The on-site installation of the sensors is shown in **Figure 10**.

Table 2. X-coordinates of the sensors in Face 8110-2110 roadway of Dongzhouyao Coal Mine.

Vibration Sensor No.	X-Coordinates (m)					Vibration Sensor No.	X-Coordinates (m)				
	Mileage 750	Mileage 813	Mileage 843	Mileage 907	Mileage 951		Mileage 750	Mileage 813	Mileage 843	Mileage 907	Mileage 951
1	0.0	1.0	0.0	0.0	0.0	13	0.0	0.0	0.0	0.0	0.0
2	2.2	3.9	2.2	2.9	2.1	14	1.8	3.2	1.8	3.2	1.7
3	4.1	7.1	4.1	5.8	4.2	15	3.7	6.4	3.7	6.7	3.6
4	5.8	10.4	5.8	8.9	7.1	16	6.3	9.5	6.3	9.5	5.7
5	8.1	12.5	8.1	12.1	8.1	17	8.5	12.5	8.5	11.6	7.9
6	10	15.8	10	15	10.1	18	10.6	15.3	10.6	14.6	10.3
7	11.9	18.5	11.9	17.5	12.3	19	12.7	18.6	12.7	17.2	12.3
8	13.9	21.6	13.9	20.7	14.3	20	14.5	20.9	14.5	20.5	14.5
9	16.2	24.4	16.2	23.7	16.2	21	16.8	24	16.8	23.9	16.5
10	17.4	27.1	17.4	26.6	18.2	22	18	27.4	18	27	18.5
11	19.3	30.2	19.3	29.6	21	23	20.2	30.1	20.2	30.2	20.7
12	21.3	33.1	21.3	32.4	22	24	22.2	33.1	22.2	33.2	22.7

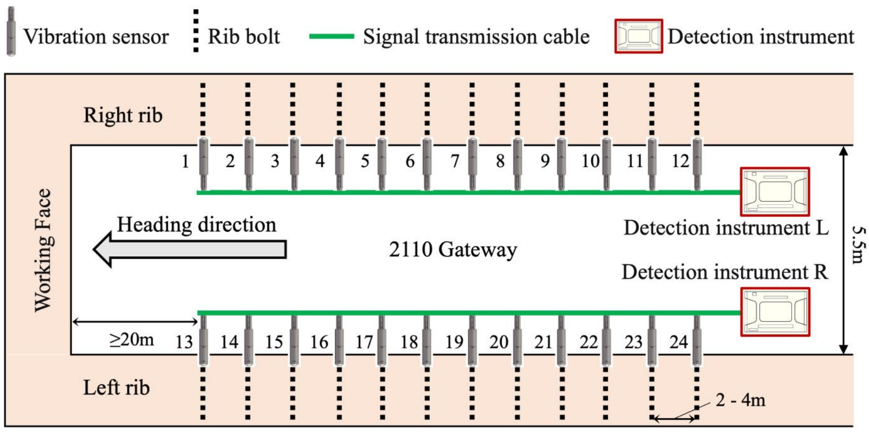

Figure 9. Vibration sensor layout plan.

Figure 10. On-site vibration sensor layout and installation photos.

4.1.3. Detection Results and Verification

Figure 11 presents the migrated imaging results obtained during advance seismic detection performed concurrently with excavation. **Figure 11a,b** shows typical imaging results acquired using the first set of sensors installed at chainage 750 m. As illustrated, two successive advance detections conducted at different excavation positions under the same sensor layout both reveal enhanced reflection energy near the fault located approximately 81.41 m ahead of reference point M16. Compared with **Figure 11a**, the imaging result in **Figure 11b**, obtained when the excavation face moved closer to the fault zone, shows a more accurately defined fault position and stronger reflection energy concentration, indicating improved imaging resolution as the source approaches the structural target. **Figure 11c,d** display imaging results corresponding to the first sensor set when the excavation advanced to chainage 813 m. Due to the shorter distance between the excavation face and the first vibration sensor, reflection energy focusing associated with the advancing face becomes more pronounced. Two main anomalous reflection zones are observed behind the excavation face, located respectively within chainage ranges of approximately 925–950 m and 1,000–1,010 m. The anomaly within chainage 925–950 m appears slightly shifted forward relative to the mapped fault position, which is interpreted to be influenced by the presence of a switch niche located near chainage 940 m, affecting wave propagation and reflection characteristics. The reflection anomaly observed within chainage 1,000–1,010 m is consistently revealed in both **Figure 11e,f**. Subsequent excavation verification, as shown in **Figure 12** confirmed the presence of a collapse column and fractured zone within the coal seam at this location, demonstrating strong agreement between seismic imaging results and actual geological conditions.

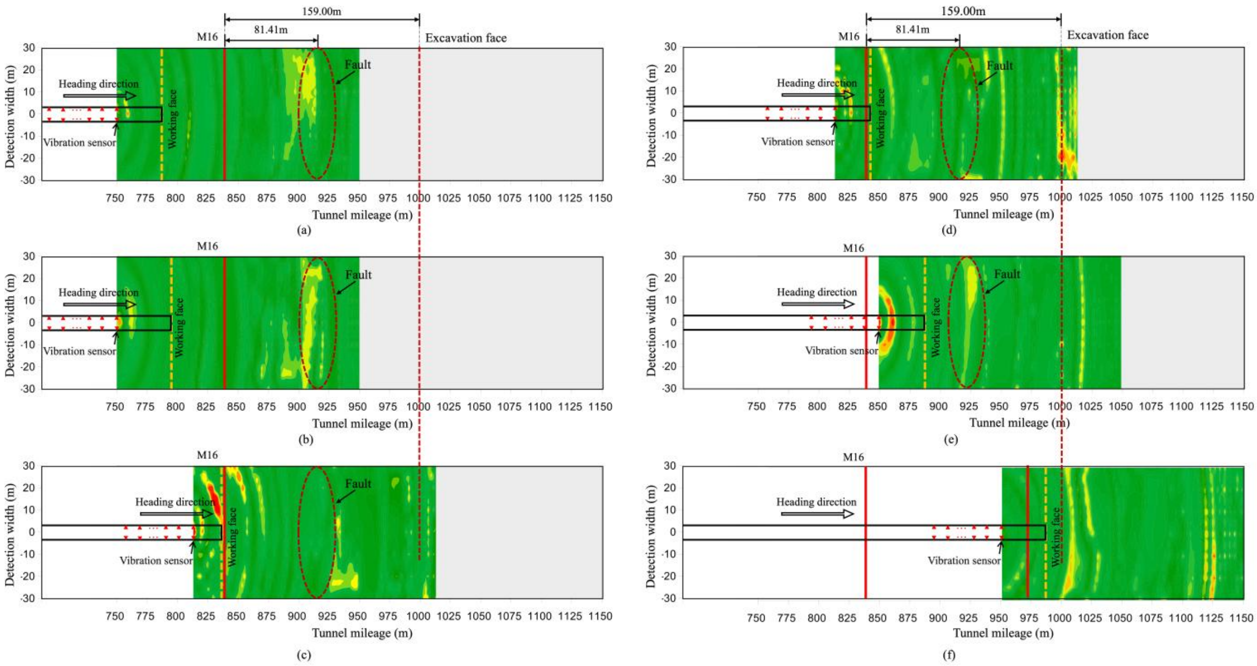

Figure 11. Variation of imaging results after migration processing during excavation.

Figure 12. Field photo of the haulage gateway at 159 m ahead of M16.

4.2. Advance Detection in Roadway 2209 of Panel 2

4.2.1. General Information

This advance detection experiment during excavation was conducted in Roadway 2209, which is located in Panel 2 of the Carboniferous C5 coal seam at Dongzhouyao Coal Mine, China. Surface elevations range from 1,293 to 1,336 m, while the roadway elevation lies between 970 and 980 m, corresponding to a burial depth of approximately 330–360 m. The ground surface is mainly covered by loess with locally developed gullies and no permanent surface water bodies, resulting in limited direct influence on underground operations. The roadway has a designed length of approximately 1,841 m with a cross-sectional dimension of 5.5 m × 3.6 m. Surrounding zones remain largely unmined, and no overlying goaf exists above the excavation area.

The C5 coal seam is nearly horizontal, with dip angles ranging from −5° to 5° and averaging approximately 4°. Coal thickness varies between 5.45 and 10.89 m, with an average value of 8.38 m. The seam exhibits a relatively complex internal structure, commonly containing 2–6 interbedded partings composed mainly of mudstone, sandy mudstone, and carbonaceous mudstone, with a cumulative thickness of approximately 1.65 m. Local structural disturbance and igneous intrusion may result in seam thinning or partial seam loss in limited zones.

Roof and floor strata are generally competent. The main roof consists of thick coarse sandstone with good integrity and relatively high strength. The immediate roof is composed of thin silty mudstone layers with comparatively weaker mechanical properties. The immediate floor is mainly siltstone, while the main floor comprises medium-grained sandstone with good structural integrity. Overall, the surrounding rock mass provides favorable conditions for roadway excavation, although local stability may decrease in structurally disturbed sections. The roof and floor conditions are detailed in the following **Table 3**.

Table 3. Roof and Floor Characteristics of Coal Seam of 2209.

Layer	Rock	Thickness (m)	Lithology Description	Compressive Strength (MPa)
Main Roof	Coarse-grained sandstone	11.55–29.5, average 20.09	Grayish-white, coarse-grained, massive structure; mainly composed of quartz and feldspar with minor gravels and loose cementation.	64.25
Immediate Roof	Silty mudstone	0.21–0.76, average 0.46	Dark gray to gray-black mudstone with massive structure and developed bedding, prone to weathering.	23.15
Immediate Floor	Siltstone	2.70–5.00, average 4.09	Grayish-white siltstone with massive structure and calcareous cementation, mainly composed of quartz and feldspar.	36.00
Main Floor	Medium-grained sandstone	3.40–6.08, average 4.73	Grayish-white medium-grained sandstone with massive structure and calcareous cementation, well cemented and relatively intact.	60.00

During roadway excavation, multiple faults, collapse columns, and localized igneous intrusions may be encountered, with some normal faults exhibiting vertical displacements of up to 20–25 m. Seismic anomaly zones identified along the alignment may correspond to seam thinning or local seam absence. Lamprophyre intrusions and collapse columns may disrupt the coal seam structure and induce fractured surrounding rock conditions, while potentially enhancing local groundwater conductivity.

Hydrogeological conditions are classified as moderate. Groundwater inflow is mainly controlled by roof sandstone fracture water and locally by structurally induced conduits. Thick mudstone strata beneath the seam act as effective aquicludes, and the calculated water inrush coefficient remains below the critical safety threshold, indicating an overall low risk of water inrush. However, localized seepage may occur within faulted or fractured zones, and advance probing together with appropriate drainage measures is therefore required during excavation.

4.2.2. Detection Test Design

The advance seismic detection procedure conducted in Roadway 2209 of Panel 2 was generally consistent with that implemented in Roadway 2110 of Panel 1. The vibration sensor layout and field installation conditions during excavation are shown in **Figure 13**.

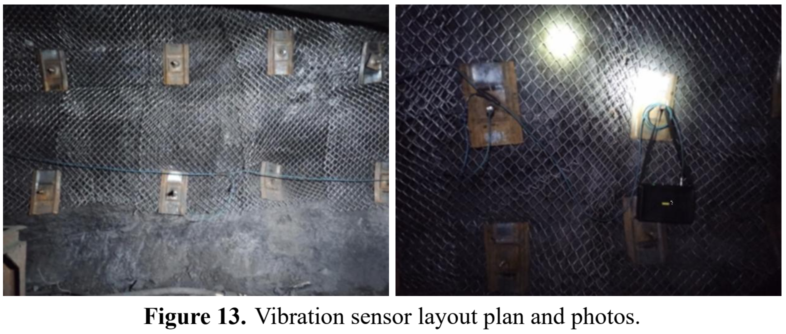

Figure 13. Vibration sensor layout plan and photos.

Prior to advance seismic detection, water-probing drilling was carried out at chainage 1,128 m in Roadway 2209 as a comparative verification measure. Three advance water-probing boreholes were arranged at the excavation face to investigate geological and hydrogeological conditions ahead of the roadway. The boreholes were deployed in a fan-shaped configuration to achieve vertical coverage of different zones in front of the excavation face.

As illustrated in **Figure 14**, Borehole No. 1 was drilled approximately along the roadway axis to identify the general occurrence of coal seams and surrounding rock ahead of the face. Boreholes No. 2 and No. 3 were inclined upward and downward, respectively, thereby providing upper and lower detection coverage. Specifically, Borehole No. 1 was drilled with an azimuth of 247° and an inclination of 0°, forming an approximately horizontal borehole with a measured depth of 85 m. Borehole No. 2 was drilled with an azimuth of 232° and an inclination of −7°, reaching a measured depth of 89 m. Borehole No. 3 was drilled with an azimuth of 262° and an inclination of −7°, also reaching a measured depth of 89 m. Together, the three boreholes formed a forward probing coverage of the excavation area, providing geological verification data for subsequent advance seismic detection and excavation safety assessment.

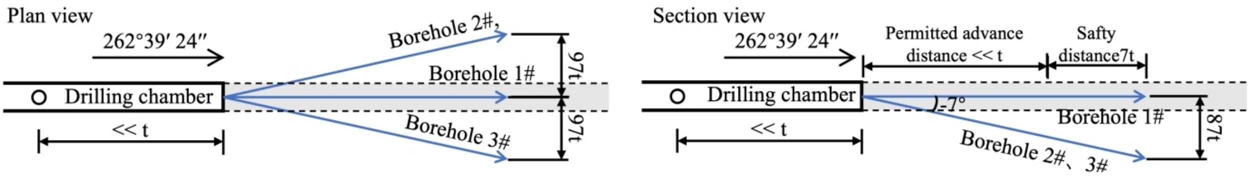

Figure 14. Layout of advance water-probing boreholes.

Note: Borehole 1#, azimuth of 262°39′, inclination of −7°, depth of 89 m; Borehole 2#, azimuth of 247°39′, inclination of 0°, depth of 85 m; Borehole 3#, azimuth of 232°39′, inclination of 7°, depth of 89 m, permitted advance distance 55 m.

4.2.3. Detection Results and Verification

Figure 15 presents a typical imaging result obtained from seismic advance detection during excavation in Roadway 2209. Three significant reflection anomalies were identified ahead of the working face, mainly located at chainages 1,186–1,206 m, 1,220–1,228 m, and 1,260–1,290 m, indicating possible geological or lithological anomalies. The borehole investigations results show as follows:

Borehole No. 1: coal (0–62 m), limestone (62–81 m), coal (81–85 m);

Borehole No. 2: coal (0–30 m), limestone (30–89 m);

Borehole No. 3: coal (0–29 m), limestone (29–89 m).

A comparison shows that the first seismic anomaly at 1,186–1,206 m corresponds closely to the limestone interval detected by drilling at 1,190–1,209 m, confirming that the anomaly is mainly caused by impedance contrasts between coal and limestone strata. This demonstrates the effectiveness of excavation seismic detection in identifying lithological changes ahead of the face. The remaining anomalies were not directly intersected by boreholes but are interpreted as potential structural or lithological disturbances requiring further verification during subsequent excavation.

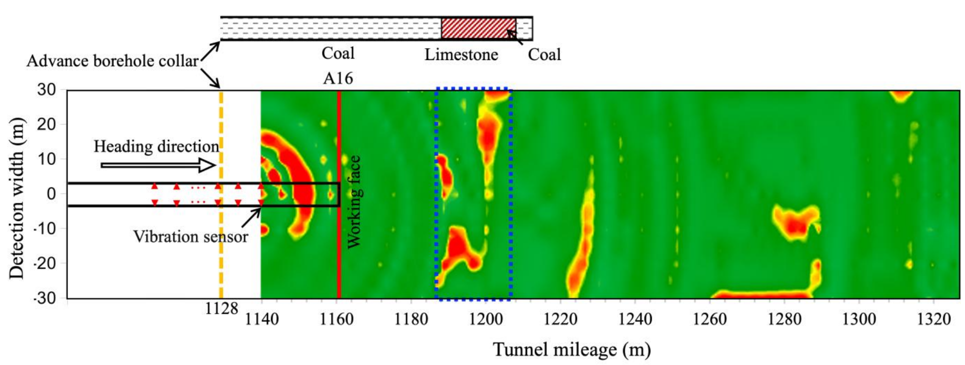

Figure 15. Imaging results after migration processing.

4.3. Integrated Analysis and Discussion

4.3.1. Physical Interpretation of Seismic Responses

The reflected seismic responses during roadway excavation are governed primarily by contrasts in elastic impedance, which is determined by the combined effects of density and seismic wave velocity. Faults, collapse columns, fractured coal–rock masses, and coal–limestone interfaces all disturb the continuity of elastic impedance and therefore generate reflected waves. In Roadway 2110, the enhanced reflection energy near the mapped fault and collapse-column zone is interpreted as the combined response of fracture-induced velocity reduction, impedance discontinuity, and wave scattering. In Roadway 2209, the strong anomaly at 1,186–1,206 m is mainly attributed to the sharp impedance contrast between coal and limestone. The gradual strengthening and spatial focusing of the reflected events as the excavation face approaches the target further indicate that the effective signal amplitude is affected by source–target distance, attenuation, and geometric spreading.

The polarity and continuity of reflection events provide additional geological information. Continuous high-amplitude events are more likely to correspond to laterally persistent lithological interfaces, whereas discontinuous or chaotic reflection patterns usually indicate fractured zones, collapse-related disturbance, or irregular structural boundaries. Therefore, the interpretation in this study was based not only on the presence of reflection energy, but also on the spatial continuity, amplitude concentration, and consistency of anomalies among repeated detections.

4.3.2. Influence of Geological Conditions

Geological conditions exert a direct influence on detection accuracy. When the target has a strong impedance contrast with the surrounding coal seam, such as a coal–limestone interface or a major fault zone, reflected energy is concentrated and the anomaly location can be constrained more reliably. By contrast, weak lithological variations within coal-bearing strata may generate low-amplitude reflections and are more difficult to interpret. Highly fractured zones may also scatter seismic energy, producing chaotic but less continuous events.

The two field cases show different but complementary geological responses. Roadway 2110 demonstrates that faults and collapse-related fractured zones can be recognized by enhanced and discontinuous reflection patterns, whereas Roadway 2209 demonstrates that lithological transitions can be identified when the coal–rock impedance contrast is sufficiently strong. This comparison suggests that the method is especially suitable for detecting major structural discontinuities and high-contrast lithological boundaries in coal roadway drivage.

4.3.3. Reliability and Quantitative Evaluation

Results from both Roadway 2110 and Roadway 2209 demonstrate that excavation seismic advance detection performs reliably under different geological conditions. In Roadway 2110, faults, collapse columns, and fractured zones were successfully detected, whereas in Roadway 2209, lithological transitions between coal and limestone were clearly identified. These cases indicate that the method is sensitive to both structural disruptions and lithological variations.

Table 4 presents a quantitative comparison between seismic prediction and field verification. The two field cases provide complementary validation conditions: Roadway 2110 mainly verifies structural anomalies by excavation exposure, whereas Roadway 2209 verifies lithological changes by advance drilling. Although the available engineering verification data are limited by mining safety and production constraints, the comparison demonstrates meter-scale consistency between the predicted seismic anomalies and the verified geological targets.

The quantitative results indicate that the proposed method can identify major geological anomalies within an engineering-acceptable error range. For the mapped fault in Roadway 2110, repeated detections constrained the anomaly before exposure, with a positioning deviation of approximately 6–10 m. For the coal–limestone transition in Roadway 2209, the first seismic anomaly overlapped well with the drilling-confirmed limestone interval, and the boundary deviation was generally less than about 5 m. These results are considered sufficient for advance warning and support adjustment in roadway drivage, where the objective is to identify hazardous zones before the excavation face reaches them rather than to produce a high-resolution stratigraphic model.

Table 4. Quantitative comparison between seismic imaging results and field verification.

Case	Predicted Seismic Anomaly	Verification Data	Estimated Positioning Error	Interpretation
Roadway 2110	Fault-related reflection near the mapped fault ahead of M16; collapse/fractured-zone anomaly around chainage 1,000–1,010 m	Subsequent excavation exposure and field geological mapping	Fault: approx. 6–10 m; collapse/fractured zone: consistent with exposed section	Structural discontinuity and fractured coal–rock mass
Roadway 2209	Major anomaly at chainage 1,186–1,206 m	Boreholes indicate limestone interval at chainage 1,190–1,209 m	Generally <5 m at the anomaly boundary	Coal–limestone lithological transition
Overall	Repeated high-energy reflection zones under different source–receiver positions	Excavation exposure and drilling verification	Meter-scale consistency for major anomalies	Reliable for advance warning and support adjustment

5. Discussion and Limitations

Compared with conventional controlled-source tunnel seismic prediction methods, the while-excavation seismic method does not require blasting, hammer excitation, or production stoppage, which gives it clear operational advantages in underground coal mines. Compared with TBM-based seismic-while-drilling studies, the present roadheader-based coal roadway environment involves lower source repeatability, stronger mining noise, and more restricted sensor installation conditions. Therefore, direct transplantation of conventional TSP or TBM-SWD processing is insufficient, and an engineering-adapted workflow is required for coal roadway excavation [14,15,23–25].

The advantage of the proposed method is its compatibility with continuous drivage and its ability to provide repeated anomaly warnings as the excavation face advances. The main disadvantage is that the source is not actively controlled, which makes data quality more dependent on the cutting state and receiver coupling. Thus, the method should be regarded as complementary to drilling, electrical, electromagnetic, and radar methods. Its greatest value lies in providing continuous, non-interruptive seismic information to guide where more targeted verification or support reinforcement should be implemented.

During roadway excavation advance detection, the monitoring environment is inherently dynamic, strongly disturbed, and constrained by limited acquisition conditions, which makes a certain degree of uncertainty unavoidable in the imaging results. Although repeated acquisition, cross-correlation-based signal extraction, preprocessing enhancement, and iterative velocity-model updating were employed in this study to reduce such uncertainty, the method may still show reduced capability in identifying anomalies under weak lithological contrast conditions, where the impedance contrast across interfaces is limited and the reflected response is intrinsically weak. Moreover, under complex three-dimensional structural conditions, the imaging results may still suffer from positioning errors or simplified interface geometry due to the limitations of two-dimensional acquisition geometry, finite receiver aperture, and multipath wave propagation. Therefore, the interpretation results should still be evaluated together with drilling verification, geological mapping, and other auxiliary information.

6. Conclusions

This study developed and validated a seismic advance detection method performed concurrently with roadway excavation in underground coal mines. By utilizing vibrations generated by roadheaders as seismic sources, continuous advance detection and imaging of geological structures ahead of excavation faces were achieved without interrupting production.

1. Signal preprocessing procedures, including time-window selection, band-pass filtering, first-arrival picking, and cross-correlation processing, effectively enhanced signal quality and enabled reliable extraction of reflection information from random excavation-induced signals. Combined with iterative velocity analysis and depth migration imaging, accurate delineation of geological anomalies was achieved.
2. Field applications conducted in Roadway 2110 and Roadway 2209 of Dongzhouyao Coal Mine demonstrated that the proposed method successfully identified faults, collapse columns, fractured zones, and lithological transitions ahead of excavation faces. Quantitative comparison showed that the major fault-related

anomaly in Roadway 2110 had a positioning deviation of approximately 6–10 m, while the coal–limestone transition in Roadway 2209 showed a boundary deviation of generally less than about 5 m compared with drilling verification. These results confirm the reliability and stability of the technique under different geological conditions.

3. The proposed while-excavation seismic advance detection method enables continuous, real-time geological forecasting without interrupting excavation operations, significantly improving construction safety and efficiency. The method exhibits strong potential for widespread application in intelligent coal mine roadway development and advance geological hazard prevention.

Author Contributions

Conceptualization, C.Z.; methodology, S.C. and F.T.; field case, D.F. and C.Z.; data curation, D.F. and C.Z.; visualization, S.C.; instrumentation, C.L.; writing—original draft, F.T.; writing—review and editing, C.Z. and S.C. All authors have read and agreed to the published version of the manuscript.

Funding

This work was supported by CHN Shenhua Energy Co., Ltd., Shendong Coal Branch (Grant No. E210100720).

Institutional Review Board Statement

Not applicable.

Informed Consent Statement

Not applicable.

Data Availability Statement

Some or all data, formulations, or codes generated or used during the study are available from the corresponding author by request. The data contain sensitive information about the mining operations and related parties that could potentially compromise the security and competitive position of the mining company involved. Access to such data is subject to strict regulations and agreements that prevent us from sharing the raw data outside of the research context.

Acknowledgments

The authors extend their sincere appreciation to the supporters for their essential support throughout this research initiative. The provision of specialized field access, technical resources, and domain expertise proved indispensable to the successful execution of this study.

Conflicts of Interest

The authors declare no conflict of interest.

AI Use Statement

The authors declare that no artificial intelligence (AI) tools were used in the preparation of this manuscript.

References

[1] Yang, M., 2025. Study on the characteristics of high-frequency electromagnetic wave detection in goaf areas along coal seam borehole. Journal of Environmental & Earth Sciences. 7(7), 259–271. DOI: https://doi.org/10.30564/jees.v7i7.9977

[2] Hanson, D.R., Vandergrift, T.L., DeMarco, M.J., et al., 2002. Advanced techniques in site characterization and mining hazard detection for the underground coal industry. International Journal of Coal Geology. 50(1–4), 275–301. DOI: https://doi.org/10.1016/S0166-5162(02)00121-0

[3] Francke, J., 2012. A review of selected ground penetrating radar applications to mineral resource evaluations. Journal of Applied Geophysics. 81, 29–37. DOI: https://doi.org/10.1016/j.jappgeo.2011.09.020

[4] Hatherly, P., 2013. Overview on the application of geophysics in coal mining. International Journal of Coal Geology. 114, 74–84. DOI: https://doi.org/10.1016/j.coal.2013.02.006

[5] Liu, X., Fan, D., Tan, Y., et al., 2021. New detecting method on the connecting fractured zone above the coal face and a case study. Rock Mechanics and Rock Engineering. 54(8), 4379–4391. DOI: https://doi.org/10.1007/s00603-021-02487-y

[6] Niu, G., Zhang, K., Yu, B., et al., 2019. Experimental study on comprehensive real-time methods to determine geological condition of rock mass along the

boreholes while drilling in underground coal mines. Shock and Vibration. 2019(1), 1045929. DOI: https://doi.org/10.1155/2019/1045929

[7] Zhang, P., Li, S., Qiu, S., et al., 2021. Advance detection technology and development of fast intelligent roadway drivage. Journal of China Coal Society. 46(7), 2158–2173. Available from: https://https://www.mtxb.com.cn/en/article/id/e9e42f25-46a8-4f31-91b1-072987d4cd37

[8] Li, S., Zhang, P., Hu, X., et al., 2024. Seismic monitoring technology of driving and detection integrated of coal mine roadway. Journal of Physics: Conference Series. 2895(1), 012055. DOI: https://doi.org/10.1088/1742-6596/2895/1/012055

[9] Zhang, P., Li, S., Guo, L., 2023. Study on time function of seismic source and numerical simulation data impulse processing of seismic while driving in mining. Coal Science and Technology. 51(1), 361–368. (in Chinese)

[10] Li, S., Zhang, P., Hu, X., et al., 2024. Full waveform inversion method for roadways based on wave velocity structure correction and regularization constraints. IEEE Transactions on Geoscience and Remote Sensing. 62, 1–14.

[11] Lu, T., Liu, S.D., Wang, B., et al., 2017. A review of geophysical exploration technology for mine water disaster in China: Applications and trends. Mine Water and the Environment. 36(3), 331–340. DOI: https://doi.org/10.1007/s10230-017-0467-z

[12] Yue, J.H., Zhang, H., Yang, H., et al., 2019. Electrical prospecting methods for advance detection: Progress, problems, and prospects in Chinese coal mines. IEEE Geoscience and Remote Sensing Magazine. 7(3), 94–106.

[13] Johnson-D'Appolonia, W.J., 2003. Applications of the electrical resistivity method for detection of underground mine workings. In Proceedings of Geophysical Technologies for Detecting Underground Coal Mine Voids, Lexington, KY, USA, 28–30 July 2003. Available from: https://https://dappolonia.com/wp-content/uploads/2022/09/22Applications-of-the-Electrical-Resistivity-Method-for-Detection-of-Underground-Mine-Workings22.pdf

[14] Taylor, N., Merriam, J., Gendzwill, D., et al., 2001. The mining machine as a seismic source for in-seam reflection mapping. In Proceedings of the SEG International Exposition and 71st Annual Meeting, San Antonio, TX, USA, 9–14 September 2001; pp. 1365–1368. DOI: https://doi.org/10.1190/1.1816352

[15] Petronio, L., Poletto, F., Schleifer, A., 2007. Interface prediction ahead of the excavation front by the tunnel-seismic-while-drilling (TSWD) method. Geophysics. 72(4), G39–G44. DOI: https://doi.org/10.1190/1.2740712

[16] Lu, B., Cheng, J., Hu, J., et al., 2011. Seismic features of vibration induced by mining machines and feasibility to be seismic sources. Procedia Earth and Planetary Science. 3, 76–85. DOI: https://doi.org/10.1016/j.proeps.2011.09.068

[17] Li, S., Zhang, P., 2021. Processing of random roadway source signals based on a cross-correlation algorithm in the deconvolution domain. Exploration Geophysics. 52(1), 98–108. DOI: https://doi.org/10.1080/08123985.2020.1768798

[18] Liu, Q., 2021. Noise attenuation based on L1-norm constraint inversion in seismic while drilling. Journal of China Coal Society. 46(8), 2699–2705. (in Chinese)

[19] Biondi, B., Sava, P., 1999. Wave-equation migration velocity analysis. In Proceedings of the 69th Annual International Meeting of the Society of Exploration Geophysicists, Houston, TX, USA, 31 October–5 November 1999; pp. 1723–1726. DOI: https://doi.org/10.1190/1.1820867

[20] Fomel, S., 2003. Time-migration velocity analysis by velocity continuation. Geophysics. 68(5), 1662–1672. DOI: https://doi.org/10.1190/1.1620640

[21] Zhu, J., Lines, L.R., Gray, S.H., 1997. Smiles and frowns in migration/velocity analysis. Geophysics. 63(4), 1200–1209. DOI: https://doi.org/10.1190/1.1444420

[22] Du, Y., Willis, M.E., Stewart, R.R., 2015. Vertical seismic profile migration velocity analysis via residual moveout in common image gathers. Geophysics. 80(5), U61–U72. DOI: https://doi.org/10.1190/geo2014-0240.1

[23] Ashida, Y., 2001. Seismic imaging ahead of a tunnel face with three-component geophones. International Journal of Rock Mechanics and Mining Sciences. 38(6), 823–831. DOI: https://doi.org/10.1016/S1365-1609(01)00047-8

[24] Petronio, L., Poletto, F., 2002. Seismic-while-drilling by using tunnel boring machine noise. Geophysics. 67(6), 1798–1809. DOI: https://doi.org/10.1190/1.1527080

[25] Chen, L., Yang, S., Guo, L., et al., 2023. Seismic ahead-prospecting based on deep learning of retrieving seismic wavefield. Underground Space. 11, 262–274. DOI: https://doi.org/10.1016/j.undsp.2023.02.001